Structure, Activity, and Inhibition of the Carboxyltransferase β-Subunit of Acetyl Coenzyme A Carboxylase (AccD6) from *Mycobacterium tuberculosis*

Manchi C. M. Reddy, Ardala Breda, John B. Bruning,* Mukul Sherekar, Spandana Valluru, Cory Thurman, Hannah Ehrenfeld, James C. Sacchettini

Department of Biochemistry and Biophysics, Texas A&M University, College Station, Texas, USA

In *Mycobacterium tuberculosis*, the carboxylation of acetyl coenzyme A (acetyl-CoA) to produce malonyl-CoA, a building block in long-chain fatty acid biosynthesis, is catalyzed by two enzymes working sequentially: a biotin carboxylase (AccA) and a carboxyltransferase (AccD). While the exact roles of the three different biotin carboxylases (AccA1 to -3) and the six carboxyltransferases (AccD1 to -6) in *M. tuberculosis* are still not clear, AccD6 in complex with AccA3 can synthesize malonyl-CoA from acetyl-CoA. A series of 10 herbicides that target plant acetyl-CoA carboxylases (ACC) were tested for inhibition of AccD6 and for whole-cell activity against *M. tuberculosis*. From the tested herbicides, haloxyfop, an arylophenoxypropionate, showed *in vitro* inhibition of *M. tuberculosis* AccD6, with a 50% inhibitory concentration (IC$_{50}$) of 21.4 ± 1 μM. Here, we report the crystal structures of *M. tuberculosis* AccD6 in the apo form (3.0 Å) and in complex with haloxyfop-*R* (2.3 Å). The structure of *M. tuberculosis* AccD6 in complex with haloxyfop-*R* shows two molecules of the inhibitor bound on each AccD6 subunit. These results indicate the potential for developing novel therapeutics for tuberculosis based on herbicides with low human toxicity.

F atty acids are the precursors to many *Mycobacterium tuberculosis* lipids, including mycolic acids, the α-alkyl β-hydroxy branched long-chain fatty acids that are one of the main components of the *M. tuberculosis* cell wall. The first committed and rate-limiting step in fatty acid biosynthesis is the production of malonyl coenzyme A (malonyl-CoA) from acetyl-CoA and bicarbonate by the acetyl-CoA carboxylase (ACC) (1). In *M. tuberculosis*, this biotin- and ATP-dependent reaction consists of two catalytic steps. The first, biotin carboxylation, is catalyzed by the α-subunit, which contains both biotin carboxylase (BC) and biotin carboxylate carrier protein (BCCP) in one polypeptide chain. BC couples carbonate to a biotin residue covalently linked to the BCCP domain to form carboxybiotin (2). The second step is the carboxyl transfer from carboxybiotin to acetyl-CoA, catalyzed by the β-subunit, carboxyltransferase (CT) (Fig. 1).

Most bacteria, including *Escherichia coli* and *Staphylococcus aureus*, have a multisubunit ACC composed of three functional polypeptides: BC, BCCP, and CT (2), while in yeast and mammals, ACC is a single polypeptide with distinct BC, BCCP, and CT domains (3). The *M. tuberculosis* genome contains three genes annotated as BC/BCCP α-subunits (AccA1 to AccA3) and six CT β-subunits (AccD1 to AccD6) (4), which is unusual, since other bacteria generally have only 1 or 2 ACCs (2). Presumably, the multiple β-subunits reflect the ability of mycobacteria to carboxylate not only acetyl-CoA but also several other distinct substrates, including the short acyl chains that serve as intermediates in glycolipid biosynthesis (5, 6). Therefore, the presence of multiple AccA and AccD genes within the *M. tuberculosis* genome is thought to be linked to the wide variety of lipids found in *M. tuberculosis* (4, 5, 7, 8).

Of *M. tuberculosis*'s 6 CT enzymes (AccD1 to -6), only AccD4, AccD5, and AccD6 were shown to be essential for the mycobacteria's viability (6, 9, 10). Quantitative real-time PCR analysis has demonstrated that the nonessential AccD1 to -3 do not show significant changes in expression throughout *M. tuberculosis* growth

phases, while AccD4 to -6 are expressed at higher levels during the exponential growth phase (11). AccD4's function in the cell is still not known. AccD5 has been shown to be a propionyl-CoA carboxylase working with AccA3, to yield methylmalonyl-CoA as reaction product, but it is also capable of using acetyl-CoA as the substrate, with lower K_m and V_{max} (4, 12). AccD6 also has been shown to form an active ACC holoenzyme with AccA3, using acetyl-CoA as its substrate (11).

The amino acid sequence identities of AccD6 (EC 6.4.1.3; Rv2247, gene *accD6*) with the other *M. tuberculosis* AccDs range from 19% to 37% (27% for AccD1, 28% for AccD2, 19% for AccD3, 32% for AccD4, and 37% for AccD5). *M. tuberculosis* AccD6 has higher similarity to the acetyl-CoA carboxylase β-subunit (AccB) and propionyl-CoA carboxylase β-subunit (PccB) of *Streptomyces coelicolor*, with sequence identities of 38% and 41%, respectively.

Herbicides as ACC inhibitors. Aryloxyphenoxypropionate (FOP) and cyclohexanedione (DIM) are herbicides that target plant ACC with little human toxicity (13, 14). They have also been found to have significant activity against apicomplexan parasites that cause malaria (15) and toxoplasmosis (16). Growth inhibition of *Toxoplasma gondii* by FOP herbicides has been shown to correlate with the inhibition of its ACCs (16). The study of FOP
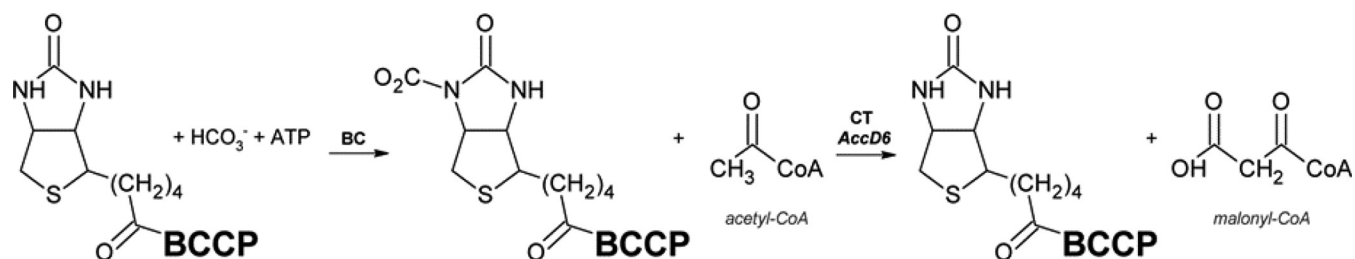
FIG 1 The reaction catalyzed by ACC proceeds in two steps. The biotin carboxylase (BC) step involves the carboxylation of a biotin molecule bound to a biotin carboxylase carrier protein (BCCP), followed by the transfer of the carboxyl moiety to an acetyl-CoA molecule, catalyzed by a carboxyltransferase (CT; *M. tuberculosis* AccD6), forming the product malonyl-CoA.

and DIM action on *T. gondii* (16), as well as on yeast gene replacement strains (17), indicates that inhibition of ACC activity leads to a complete inhibition of the organisms' growth, as in plants (18). The effect of the herbicides haloxyfop and diclofop was previously evaluated against *M. tuberculosis* AccA3-AccD6 and AccA3-AccD5 holoenzymes at a 100 μM concentration. Haloxyfop and diclofop inhibit AccA3-AccD6 complex activity by 60 and 13%, respectively (11). Diclofop was shown to inhibit AccA3-AccD5 acetyl-CoA carboxylation by 90% and propionyl-CoA carboxylation by only 30% (12). Earlier studies of the single *M. tuberculosis* AccD5 subunit demonstrated that its activity was not inhibited by diclofop and haloxyfop (5).

Cocrystal structures for CT subunits bound to substrates have been reported from a variety of species, but only the *Saccharomyces cerevisiae* CT domain crystal structure has been solved in complex with the herbicides haloxyfop (19), tepraloxydim (20), and pinoxaden (a phenylpyrazolin) (21), showing one molecule of herbicide bound to the active site.

Here we present the first structure of *M. tuberculosis* AccD6. We also characterize the ACC-inhibiting activity of the FOP herbicide haloxyfop against AccD6 and the crystal structure of *M. tuberculosis* AccD6 in complex with haloxyfop, revealing two copies of the inhibitor bound to each subunit of the AccD6 homodimer.

MATERIALS AND METHODS

Protein cloning, expression, and purification. A 1,422-bp DNA fragment containing the AccD6 gene (Rv2247) was amplified by PCR using *M. tuberculosis* H37Rv genomic DNA as a template (BEI Resources, Colorado State University). The following oligonucleotides were used as the forward and reverse primers, respectively: 5′-AGATGAAGCCATATGAC AATCATGGCCCCCCGAGGCGGTTG-3′ and 5′-AGAGTAAGCTTACA GCGGGATGTTCTTGAGGCGGCC-3′. The amplified DNA fragment was purified using the QIAquick PCR purification kit (Qiagen), following the manufacturer's protocol. The purified DNA fragment was digested with NdeI and HindIII and then ligated using the corresponding restriction sites into a pET-28b vector (Novagen) to yield an N-terminal 6× His tag recombinant vector. BL21 Star (DE3) cells were transformed with the AccD6::pET-28b vector. An overnight culture was diluted to 1:50 in fresh medium and grown to mid-log phase at 37°C in LB media (Difco). The cells were induced with 1 mM (final concentration) IPTG and grown for 16 h at 16°C.

Cells were harvested by centrifugation. The cell pellet was resuspended in 20 mM Tris-HCl (pH 7.5), 10 mM imidazole, 0.5 M NaCl, and 10% glycerol (vol/vol) containing 1 mM DNase, 1 mM MgCl₂, and Complete EDTA-free protease inhibitor cocktail (Roche). The cell suspension was lysed using a French press at 18,000 lb/in², and the resulting cell lysate was centrifuged at 15,000 × g at 4°C for 1 h. The supernatant was collected and

filtered through a 0.2-μm filter and loaded onto a HisTrap nickel chelating column (GE Healthcare). His₆-tagged AccD6 was eluted with a 0.2-liter linear gradient of 75 to 500 mM imidazole in 20 mM Tris (pH 7.5), 0.5 M NaCl, and 10% glycerol (vol/vol). The eluted protein was dialyzed overnight in a solution of 20 mM Tris (pH 7.5), 50 mM NaCl, 10% glycerol (vol/vol), and 1 mM dithiothreitol (DTT). The purified protein was concentrated to 14 mg ml⁻¹ prior to crystallization. Size exclusion chromatography confirmed that AccD6 is a two-subunit oligomer in solution (data not shown).

***M. tuberculosis* AccD6 activity assay.** AccD6 activity was monitored by measuring the reverse reaction rate (Fig. 1). Using malonyl-CoA as a substrate, the formation of acetyl-CoA was coupled to the citrate synthase-malate dehydrogenase (CS/MDH) reaction involving the reduction of NAD^+ (22). The formation of NADH, which is proportional to the activity of *M. tuberculosis* AccD6, was measured spectrophotometrically at 340 nm using a Thermo Scientific Multiscan Go plate reader. The MDH reaction was initially kept in equilibrium in the absence of AccD6. Addition of AccD6 to the reaction mix, in the presence of CS, induces oxalacetate consumption by CS and shifts the equilibrium of the MDH reaction, leading to the AccD6-dependent formation of NADH. The reaction, which was carried out in a Corning 384-well plate at 30°C, was monitored for 30 min. The 100 μl reaction mixture contained 0.6 mg ml⁻¹ BSA, 100 mM potassium phosphate (pH 8.0), 20 mM L-malic acid, 0.5 mM NAD^+, 6 mM biocytin, 3.6 U ml⁻¹ MDH, 6.8 U ml⁻¹ CS, and various concentrations of malonyl CoA (0 to 40 μM). The kinetic parameters were calculated at an enzyme concentration of 2 μM and 1% (vol/vol) dimethyl sulfoxide (DMSO). Data were fitted to the Henri-Michaelis-Menten equation (HMM):

$$v = V_{max}[S]/K_m + [S] \qquad (1)$$

in which v, V_{max}, [S], and K_m correspond to, respectively, the steady-state reaction rate, the maximum reaction rate, substrate concentration, and the HMM constant for substrate S, using the GraphPad Prism demo version for Windows (GraphPad Software, La Jolla, CA, USA).

***M. tuberculosis* AccD6 inhibition assay.** Ten commercially available herbicides, reported as ACC ligands (23), were selected for their evaluation as possible *M. tuberculosis* ACC inhibitors. The compounds tested were clodinafop, cyhalofop, haloxyfop, fluazifop, and diclofop (from the FOP family) and sethoxydim, alloxydim, cycloxydim, tepraloxydim, and tralkoxydim (from the DIM family). Their inhibitory activity against *M. tuberculosis* whole cells was evaluated against MC²-7000 strain cultures (10 ml Difco 7H9, 100 μl dextrose, 1 ml oleic acid-albumin-dextrose-catalase [OADC], 85 μl NaCl [10% solution], 25 μl Tween 80, 10 μl of malachite green [0.25 mg/ml], and 1 mM pantothenic acid), grown for 3 days, and diluted to an optical density at 600 nm (OD₆₀₀) 0.005. Each compound was tested in the 100 μM to 100 nM range. After 6 days of incubation at 37°C, culture plates were stained with resazurin and read on the 7th day. The enzymatic inhibitory activity was assessed under the conditions described in the "*M. tuberculosis* AccD6 activity assay" above, in the presence of 300 μM malonyl-CoA, and various concentrations of

each compound (10 to 2,000 μM), independently. The reaction mixtures were incubated at room temperature for 20 min and were initiated by the addition of malonyl-CoA. The dose response was measured by calculating the decrease in initial velocity, and 50% inhibitory concentrations ($IC_{50}s$) were assigned according to equation 2:

$$v_i/v_o = 1/[1 + ([I]/IC_{50})^n] \qquad (2)$$

where v_i/v_o, $[I]$, and n are enzyme fractional activity in the presence of inhibitor I, inhibitor concentration, and the Hill coefficient, respectively.

Haloxyfop-*R*-methyl synthesis. Haloxyfop-*R*-methyl (methyl ester, AK Scientific, Inc.) was hydrolyzed to the acid form. Haloxyfop-*R*-methylpropanoic acid (referred to here as haloxyfop-*R*), 2-[4-[[3-chloro-5-(trifluoromethyl)-2-pyridinyl]oxy]phenoxy] methyl ester (2R) (0.24 mmol), was dissolved in 10 ml of 2:1:1 tetrahydrofuran-CH_3OH-H_2O and then subjected to the addition of LiOH monohydrate (3.0 equivalent, 0.72 mmol, 30.2 mg). The solution was stirred overnight and then extracted with three 6-ml portions of diethyl ether. The aqueous phase was acidified to pH 1 with 2 M HCl (aq), and the resulting mixture was extracted with two 5-ml portions of ethyl acetate. The light yellow organics were dried over anhydrous $MgSO_4$ for 5 min, filtered, and concentrated *in vacuo* to afford the desired product as an analytically pure pale yellow liquid (60 mg, 69% yield). [1]H nuclear magnetic resonance (NMR) (500 MHz, CDCl$_3$) data are as follows: δ 13.15 (s, 1), 8.55 (s, 1), 8.50 (s, 1), 7.16 (d, 2), 6.92 (d, 2); 4.85 (q, 1), 1.52 (d, 3), HPLC-MS: 98% at 254 nm, MS *m/z* 360, 362 (M-H).

Isothermal titration calorimetry (ITC). An ITC200 microcalorimeter (MicroCal, Inc., Northampton, MA) was used to carry out ITC experiments. *M. tuberculosis* AccD6 at 50 μM and 2 mM haloxyfop-*R* in 20 mM Tris-HCl (pH 7.5), 50 mM NaCl were used to fill the sample cell (200 μl) and syringe (39.7 μl), respectively. The reference cell (200 μl) contained water. Thirty-six injections of ligand into macromolecule were carried out at 30°C and 500 rpm. The first injection was 0.5 μl, while the remaining injections were 1 μl each with 10-s durations and 5-min spacing. The first data point (corresponding to the first ligand injection) was not included in data analyses. Control titrations (ligand into buffer) were performed to subtract the heat of dilution and mixing for each experiment prior to data analysis. ITC data were fitted to equation 3:

$$\Delta G = \Delta H - T\Delta S = RTlnK_a \qquad (3)$$

where ΔH is the enthalpy of binding, ΔG is the Gibbs free energy change, ΔS is the entropy change, T is the absolute temperature in kelvins, R is the gas constant (1.987 cal K^{-1} mol^{-1}), and K_a is the association constant. The dissociation constant, K_d, was calculated as the inverse of K_a. Data were evaluated using Origin 7 SR4 software (MicroCal, Inc.).

Crystallization, data collection, and refinement. Initial crystallization screening of *M. tuberculosis* AccD6 was performed via the sitting drop method using the Crystal Screen I and II, Index, SaltRx (Hampton Research), and Wizard I and II (Emerald Biosciences) screening kits. Crystals were grown by mixing 3 μl of protein solution with 2 μl of well solution and equilibrated by hanging-drop vapor diffusion at 295 K in 24-well Linbro trays containing 500 μl well solution. Crystals were obtained in 5 to 7 days. Apo AccD6 was crystallized in 60% Tacsimate. The apo crystals were flash-cooled with Paratone N (Hampton Research, Laguna Niguel, CA), and the X-ray diffraction data were collected at the Advanced Photon Source 23-ID beam line using a MAR 300 charge-coupled device (CCD) detector (MarMosaic; Marresearch). HKL2000 (24) was used to integrate and scale the diffraction data. Examination of the diffraction data disclosed that the crystals were twinned in a pseudomerohedral manner, and the correct space group was P2$_1$2$_1$2$_1$. The test for pseudomerohedral twinning was accomplished using phenix.xtriage, and phenix.refine was used to refine twinned data with a twin law of $k,h,-l$. Diffraction images also exhibited anisotropy and ellipsoidal truncation. Anisotropic scaling was performed on the data prior to refinement (25).

The structure of apo AccD6 was solved by molecular replacement as implemented in PHASER (University of Cambridge, United Kingdom)

TABLE 1 Crystallographic statistics for the *M. tuberculosis* AccD6 apo and haloxyfop-*R* complex structures

Parameter	Apo	Haloxyfop-*R*
Data collection		
Space group	P2$_1$2$_1$2$_1$	I222
Resolution	50–3.0	63–2.3
Twin fraction	0.48	NA
Unit cell *a*, *b*, *c* (Å)	82.3 × 82.4 × 157.9	117.8 × 126.2 × 161.7
Redundancy	11.9 (8.7)	7.0 (6.3)
Observations	20,652	54,918
Observations test set	1,096	1,996
Completeness (%)	97.8 (90.4)	100 (99.0)
R_{merge}	15.2 (88.1)	7.80 (3.90)
R_{pim}	0.02 (0.11)	0.01 (0.14)
$I/I\sigma$	29.5 (2.83)	12.9 (2.70)
Refinement		
R_{work}	23.7	16.6
R_{free}	30.4	19.8
No. of atoms		
Protein	6,221	6,483
Solvent	5	552
Ligand (including ions)	0	95
Ramachandran analysis		
Most favorable + allowed (%)	95.9	99.8
Root mean square deviation		
Bond lengths (Å)	0.008	0.007
Bond angles (°)	1.227	1.118

(26). The complete PccB protein from *S. coelicolor* (PDB accession code 1XNV) (25) was used as a search model with water and ions removed.

For the formation of the AccD6 inhibitor complexes, haloxyfop-*R* dissolved in DMSO as a 100 mM stock solution was added to the concentrated protein solution at a molar ratio of 5:1 and incubated for 1 h at 16°C. The haloxyfop-*R* complex was crystallized with 3.5 M sodium formate. Crystals were transferred directly to a cryoprotectant (30% ethylene glycol; Hampton Research) and flash-cooled in a liquid nitrogen stream at 100 K before data collection.

AccD6-haloxyfop-*R* diffraction data were collected at the Advanced Light Source Beamline 5.0.2 (Lawrence Berkeley National Laboratory, Berkeley, CA) with a Quantum 315 charge-coupled device detector. The HKL2000 program package was used for integration and scaling of the haloxyfop-bound crystals. The AccD6 haloxyfop-*R* complex structure was solved by molecular replacement using PHASER with chain A of the apo AccD6 structure as a search model. All refinement was performed by PHENIX (26) with intermittent manual model building done in COOT (27). Refinement statistics are summarized in Table 1. Geometry of the models was assessed with MOLPROBITY (28). All pictures were rendered with PyMol (29).

Protein structure accession numbers. Structures were deposited in the Protein Data Bank with the accession codes 4FB8 (for the apo structure) and 4G2R (for the haloxyfop-*R* bound structure).

RESULTS AND DISCUSSION

M. tuberculosis **AccD6 activity and inhibition assays.** *M. tuberculosis* AccD6 activity was measured in the coupled malate dehydrogenase and citrate synthase assay that follows the formation of NADH at 340 nm (22). For the purified recombinant *M. tuberculosis* AccD6, the K_m for malonyl-CoA was calculated to be 390 ±
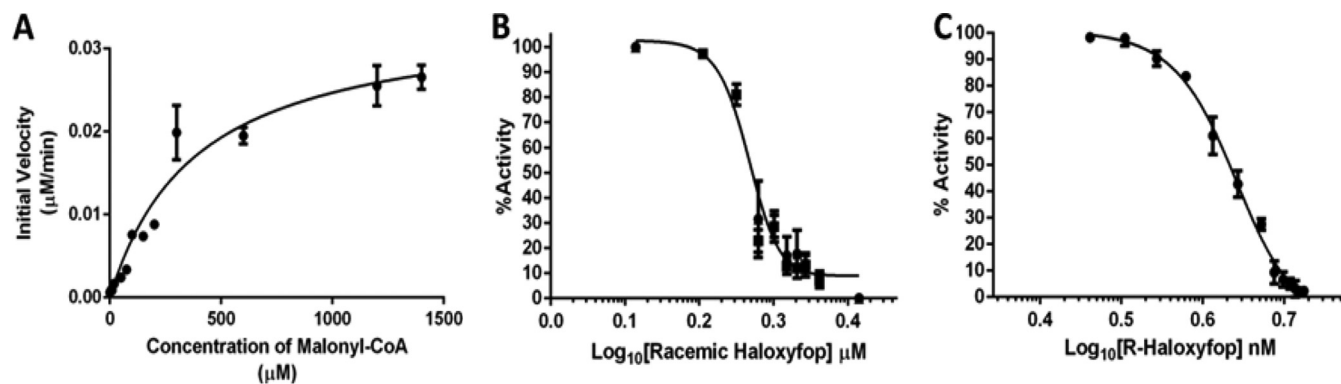
FIG 2 *M. tuberculosis* AccD6 *in vitro* assays. (A) Reaction velocity plotted versus malonyl-CoA concentration ($K_m = 390 \pm 70 \, \mu M$; $V_{max} = 5.5 \pm 0.4 \, \mu M \, min^{-1}$). (B) IC$_{50}$ ($70.2 \pm 1 \, \mu M$) plot of racemic haloxyfop inhibition of *M. tuberculosis* AccD6. (C) IC$_{50}$ ($21.4 \pm 1 \, \mu M$) plot of haloxyfop-*R* inhibition of *M. tuberculosis* AccD6.

70 μM, and the V_{max} was $5.5 \pm 0.4 \, \mu M \, min^{-1}$ (Fig. 2A). The *M. tuberculosis* AccD6 K_m for malonyl-CoA is higher than K_m values described for all other CTs studied to date; for example, *E. coli* and yeast CTs have K_m values of 100 μM (30) and 75 μM (19), respectively.

Of the 20 commercially available FOP and DIM herbicides tested for their effect on *M. tuberculosis* AccD6 activity, only haloxyfop (racemic mixture) showed inhibitory activity against AccD6, with an IC$_{50}$ of $70.2 \pm 1 \, \mu M$ (Fig. 2B). It is known that only the R enantiomer, haloxyfop-*R*, has herbicidal activity, whereas the S enantiomer is essentially inactive (31). The haloxyfop-*R* enantiomer was synthesized and tested against AccD6, and it yielded an IC$_{50}$ of $21.4 \pm 1.1 \, \mu M$ (Fig. 2C) against the *M. tuberculosis* enzyme. This shows that, like for plants, the R enantiomer is the active species.

A previous study reported haloxyfop (racemic mixture) inhibiting AccA3-AccD6 complex activity (60% inhibition at a concentration of 100 μM) (11). Notwithstanding, diclofop also was reported to inhibit the AccA3-AccD6 complex (13% inhibition at 100 μM) (11), although we detected no inhibition of AccD6 at a concentration of 100 μM. Similar results have been reported for

AccD5 (5, 12). While AccA3-AccD5 was reported to be inhibited by diclofop (90% and 30% inhibition at 100 μM, using acetyl-CoA and propionyl-CoA as the substrates) (12), AccD5 was not inhibited in the presence of diclofop up to 300 μM (5). This suggests that the interactions of diclofop with AccD5 may be dependent upon the formation of a carboxylase-carboxyltransferase (AccA-AccD) complex. The same study reported that the *M. tuberculosis* AccD5 subunit is not inhibited by haloxyfop (5), despite its similarity (37% identity) to *M. tuberculosis* AccD6. The same set of herbicides showed no influence on growth when tested against *M. tuberculosis* whole cells.

Overall structure of *M. tuberculosis* AccD6. The crystal structures of apo and haloxyfop-bound *M. tuberculosis* AccD6 were determined at 3.0-Å and 2.3-Å resolutions, respectively (Fig. 3A to C). The atomic model of both the structures is in agreement with the X-ray diffraction data and the expected value for geometric parameters (Table 1). Unlike the hexameric ring-shaped architecture found in the assembly of *M. tuberculosis* AccD5 (5), AccD6 is a homodimer resembling the yeast and *E. coli* ACC CT domains. Each subunit of the homodimer is comprised of 473 amino acids. Thirteen residues of the N terminus and 25 residues of the C
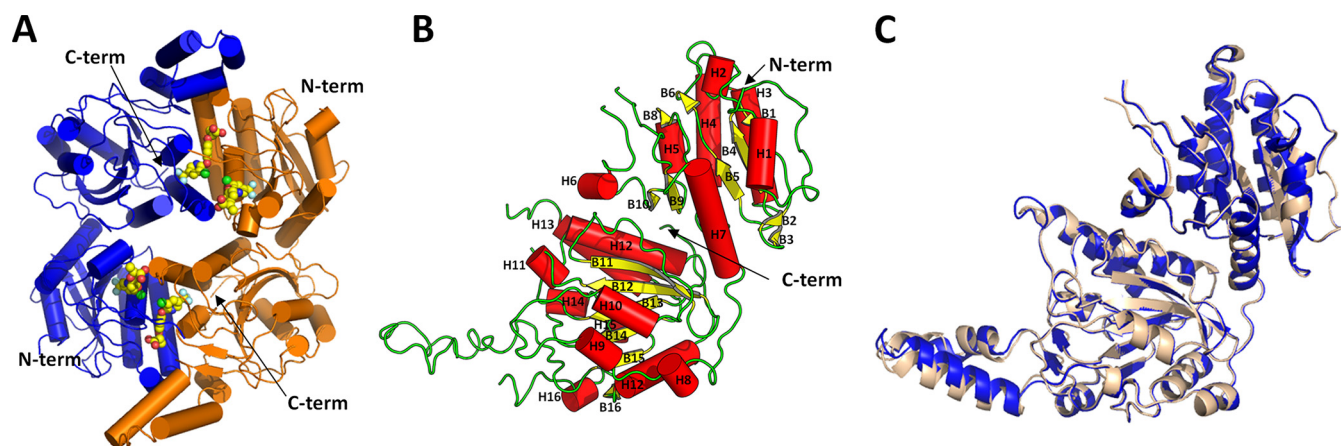

FIG 3 Ribbon diagram of *M. tuberculosis* AccD6. (A) Ribbon diagram of the two subunit AccD6 holoenzyme, with the haloxyfop ligands depicted as sticks and balls. Subunits are depicted by differences in color, both colored by secondary structure. Subunit 1 is in blue and subunit 2 is yellow. (B) Ribbon diagram (colored by secondary structure) of the apo AccD6 single subunit. (C) Superimposition of *M. tuberculosis* AccD5 subunit 1 (blue) and subunit 2 (tan). Cα RMSD, 1.0 Å. Subunits are shown as ribbons.
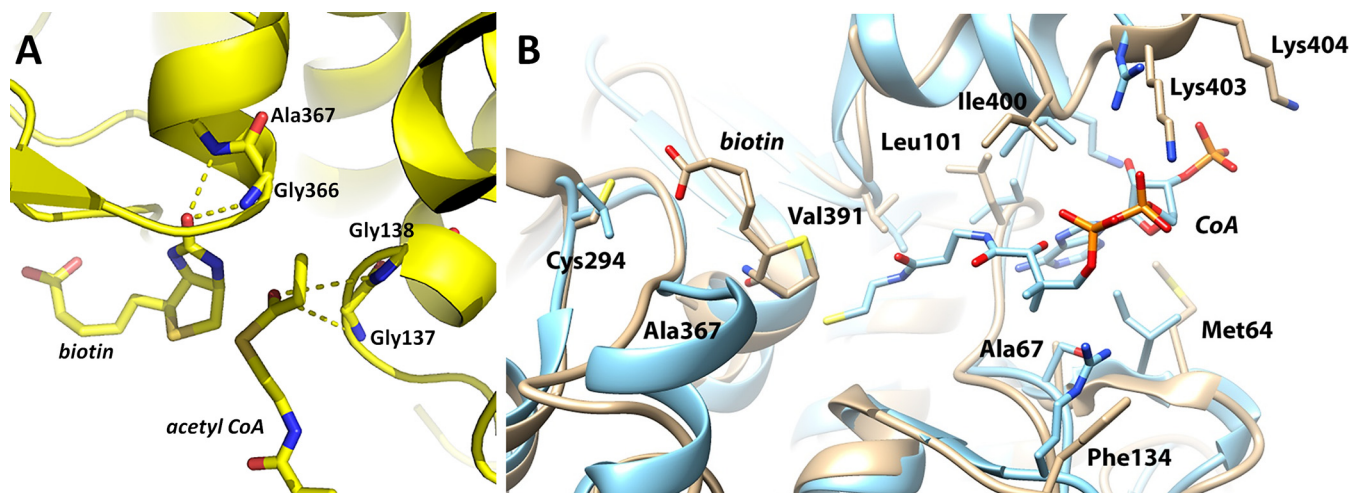
FIG 4 *M. tuberculosis* AccD6 active site. (A) Two sets of oxyanion-stabilizing residues are highly conserved among the CT domains of different species, including the NH of Gly137 and Gly138 and the NH of Gly336′ and Ala367′. The structural similarity strongly suggests a similar enzyme mechanism. (B) Comparison of the *M. tuberculosis* AccD6 and yeast ACC (PDB code 1OD2) active sites. The yeast structure is in blue, while the *M. tuberculosis* structure is in tan and biotin is in tan. Side chains within 4 Å of each ligand are depicted as sticks.

terminus in each subunit were not modeled due to disorder in both structures. The protein has a mixed α/β fold with a total of 17 α-helices and 16 β-strands that resemble the crotonase family fold (32, 33) (Fig. 3B). Each subunit of the dimer consists of two domains: the N-terminal domain (α-helices 1 to 7 and β-strands 1 to 10) and the C-terminal domain (helices 8 to 17 and β-strands 11 to 16). H4 and H5 of the N-terminal domain of one subunit and H13 and H14 of the C-terminal domain of the second subunit (Fig. 3A) form the dimer interface. Both subunits contain a β-sheet flanked on each side by α-helices.

Comparison of *M. tuberculosis* AccD6 to other CT domains. A subunit of the *M. tuberculosis* AccD6 (chain A, 435 residues from Apo AccD6; PDB code 4FB8) was compared to both the eukaryotic (human, PDB code 3FF6, and yeast, PDB code 1UYT) and prokaryotic (*E. coli*, PDB code 2F9Y, and *S. coelicolor*, PDB codes 1XNV and 3MFM) CT domain structures using CaspR (34). Despite an overall sequence identity of about 20% between the enzyme from *M. tuberculosis* and the eukaryotic CT domains, all structures exhibit the same general fold. Superposition showed that the *M. tuberculosis* AccD6 has root mean square differences for Cα (Cα RMSD) of about 1.4 Å with the human CT domain (chain A) (35) and 1.4 Å with the yeast CT domain (chain A) (19). *M. tuberculosis* AccD6 aligned with *S. coelicolor* PccB (41% sequence identity [36]) and AccB (38% sequence identity [37]), showing Cα RMSD of 1.7 Å and 1.69 Å.

E. coli AccD is a heterodimer with an α2β2 subunit composition (38). *M. tuberculosis* AccD6 has Cα RMSD of 1.7 Å and 1.9 Å in comparison to the *E. coli* N-terminal domain of the β-subunit and the α-subunit C-terminal domain. In comparison to *M. tuberculosis* AccD6, the N terminus of the *E. coli* CT domain contains a 30-residue extension shown to be a zinc finger domain (38). The zinc finger domain is proposed to act as a lid that closes upon substrate binding in the active site (38) and has been detected in all of the prokaryotic ACC enzymes studied to date. Similar to eukaryotic ACCs, *M. tuberculosis* AccD6 does not contain a zinc finger motif.

M. tuberculosis AccD6 substrate binding pocket. Alignment

of the *M. tuberculosis* AccD6 structure with the previously reported β-subunit of ACC from *S. coelicolor* in complex with acetyl-CoA (39) allowed us to model the binding and interactions of acetyl-CoA and biotin with active site residues. The *M. tuberculosis* AccD6 active site is formed by the dimer interface, as shown in Fig. 3A. This interface provides contacts that are essential for substrate specificity, catalysis, and protein stability, being highly conserved among biotin-dependent carboxyltransferases (36).

Both the acetyl-CoA binding pockets and the biotin pockets are located at the interface between the N-domain of one monomer and the C-domain of its dimeric partner. In *S. coelicolor* ACC, the key catalytic residue consists of two pairs of oxyanion-stabilizing residues (the oxyanion holes). Gly419 and Ala420 hydrogen bond with the carbonyl group of biotin, whereas Gly182 and Gly183 hydrogens bond with the carbonyl group of acetyl-CoA. These four residues are highly conserved among the CT domains of different species, including *M. tuberculosis* AccD6 (Gly336, Ala367, Gly137, and Gly138) (Fig. 4A).

Given the high degree of sequence homology in the active site of *M. tuberculosis* AccD6 and those of other ACCs, it is very likely that the substrate binding is highly conserved. The entrance to the active site is an opening which measures approximately 8 Å by 14 Å on the surface and leads to a cavity of approximately 400 Å^3. The cavity is defined by alpha helices H2, H5, and H14 as well as the loop between β15 and H16 and expands to allow substrate binding. A model of the substrate in the active site indicates that the adenine and phosphate moieties of the substrate are likely solvent exposed, making contacts with polar residues from the surface of the protein and the acyl portion of acetyl-CoA inserts into the cavity of the protein. The adenine moiety lies next to the loop preceding β-strand 15 and the loop preceding H4′ and H2′ (the prime designates the other subunit in the dimer). The adenine NH$_2$ extension is poised to hydrogen bond with the backbone oxygen of Ala99, while the adenine N7 atom is in position to hydrogen bond with Met64. The phosphate oxygen atoms of acetyl-CoA are positioned to form electrostatic interactions with Lys401, Lys403, and Lys404. The terminal carbonyl oxygen atom
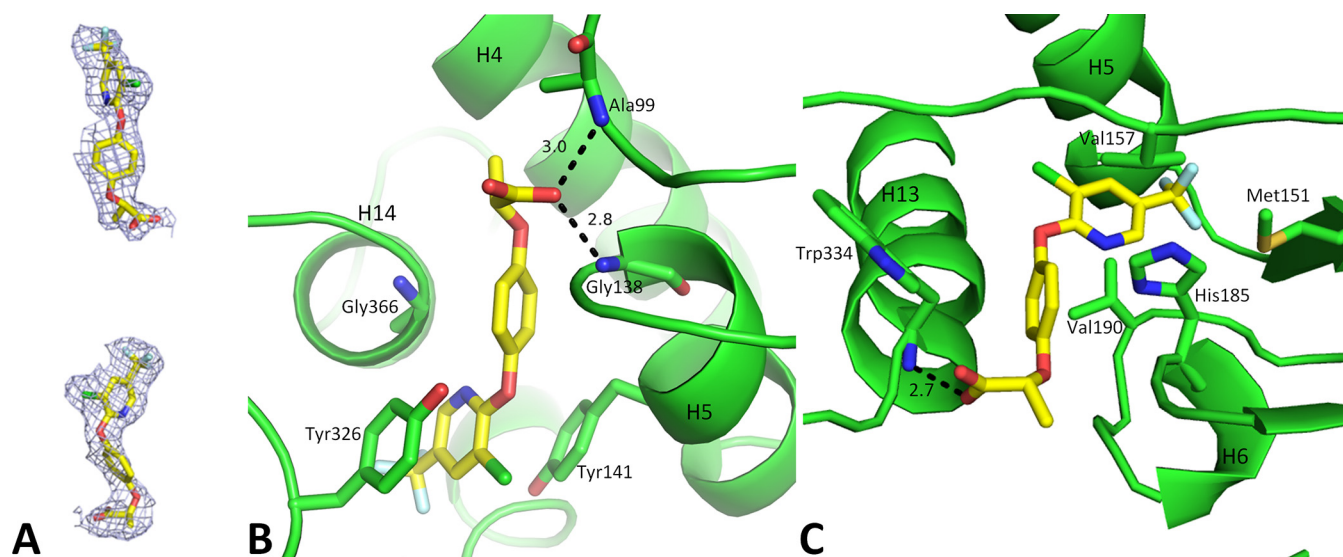
FIG 5 (A) Electron density of haloxyfop (yellow sticks) and composite OMIT map electron density (blue contoured at 1 σ). (B) Haloxyfop interaction with *M. tuberculosis* AccD6 binding site 1; (C) haloxyfop interaction with *M. tuberculosis* AccD6 at binding site 2. Haloxyfop is in yellow, and protein side chains are in green. Dashed lines represent hydrogen bonds, and numbers represent distances, in Å.

fits into an oxyanion hole composed of the backbone nitrogen atom of Gly131 and the nitrogen atom of the tetrahydrothiophene ring of the biotin molecule. The biotin substrate lies deeper in the cavity, next to the acyl-CoA chain, and is largely buried.

The active site organization is conserved in other CT domains, such as that of *S. aureus* (38), as well as in the β-subunit of ACC from *S. coelicolor* (39) and *S. cerevisiae* (40) in complex with acetyl-CoA. The crystal structure of the yeast CT in complex with acetyl-CoA shows the ligand binding site resides between the N-terminal domain of one subunit and the C-terminal domain of another subunit in the dimer interface (40). There are minor differences in the N7 position of acetyl-CoA, which hydrogen bonds with Lys1592 in the yeast structure, versus Met64 in the *M. tuberculosis* structure. A significant difference is the charged residues that interact with the phosphate groups of CoA: Lys403 and Lys404 side chains in the *M. tuberculosis* AccD6 structure (Fig. 4B) and Arg2036 and Arg2037 in the yeast CT structure.

***M. tuberculosis* AccD6 haloxyfop-*R* complex.** The crystal structure of AccD6 cocrystallized with a 3-fold molar excess of haloxyfop-*R* shows two molecules of inhibitor bound per subunit of AccD6. Electron density for the bound inhibitor is shown in Fig. 5A. The structure of other ACC-inhibitor complexes describe the binding of only one molecule per subunit, and this is the first time a second inhibitor binding site is observed bound to an ACC. Both haloxyfop-*R* binding sites are located at the subunit interface. The first binding site (designated site 1) is located in a cleft that partially overlaps with the active site (Fig. 5B). The second binding site (site 2) is an adjacent pocket with no described function (Fig. 5C). The first site is connected to the second site by a small channel approximately 6 Å in diameter and 5 Å in length.

Comparison of the haloxyfop-bound AccD6 to the apo form shows that the main differences between the two structures are located on the residues and secondary structural elements surrounding both haloxyfop binding sites (superimposition of the apo and haloxyfop bound structures reveals a Cα RMSD of 1.0 Å). Haloxyfop binding site 1 is formed by three helices encompassing

H13, H14, and H5′. In site 1, the carboxyl end of haloxyfop is near the protein surface, while the trifluoromethylpyridyl is buried deeper to allow hydrophobic contacts. The trifluoromethylpyridyl group is sandwiched between the aromatic side chains of Tyr141 and Tyr326. The phenyl ring in the center of haloxyfop makes van der Waals contacts with Gly366 and Gly137, while the trifluoroethyl group makes hydrophobic interactions with Tyr326. In site 1, the carboxylate group of haloxyfop forms hydrogen bonds with the backbone amides of Gly138 (2.84 Å) and Ala99 (2.85 Å) (Fig. 6A).

The haloxyfop binding site 2 (Fig. 5C) is formed by the C-terminal region of H13, H6′, the N-terminal loop of H6′, the C-terminal loop to β-strand 9, and H5′. This site is similar to site 1 in that it contains a solvent-exposed carboxyl group and a trifluoromethylpyridyl ring that is buried deeper in the hydrophobic environment of the protein. The trifluoromethylpyridyl ring forms hydrophobic contacts with Val157. The phenyl ring in the center of haloxyfop makes van der Waals and hydrophobic contacts with Trp334, Val190, and Ser188. In site 2, haloxyfop makes only one hydrogen bond: the carboxyl group to the backbone amide of Trp334 (2.7 Å). The methyl group is positioned to make hydrophobic contacts with His184 (Fig. 6B).

At site 1 (Fig. 5B), Tyr141 and Tyr326 rotate to accommodate the stacking interactions with haloxyfop. The phenyl ring in the center of haloxyfop in site 1 forces H5 outward (approximately 1.5 Å) in comparison with the apo structure, while the carboxyl group forces the loop between β6 and H4 (bearing residue Ala99) outward by 1.1 Å. At haloxyfop binding site 2 (Fig. 5C), the haloxyfop phenyl ring in the center displaces H6 by 2.1 Å. Both rings of the haloxyfop in site 2 shift the loop between β9 and H5 (bearing residue Val157) outward in comparison to the apo structure (by approximately 1.3 Å). The trifluoromethyl group of haloxyfop at site 2 is located near Met151, which adopts a different rotamer conformation than in the apo structure; β9 also shifts approximately 1.3 Å.

Structural basis of *M. tuberculosis* AccD6 inhibition. Haloxyfop occupies the *M. tuberculosis* AccD6 substrate binding site
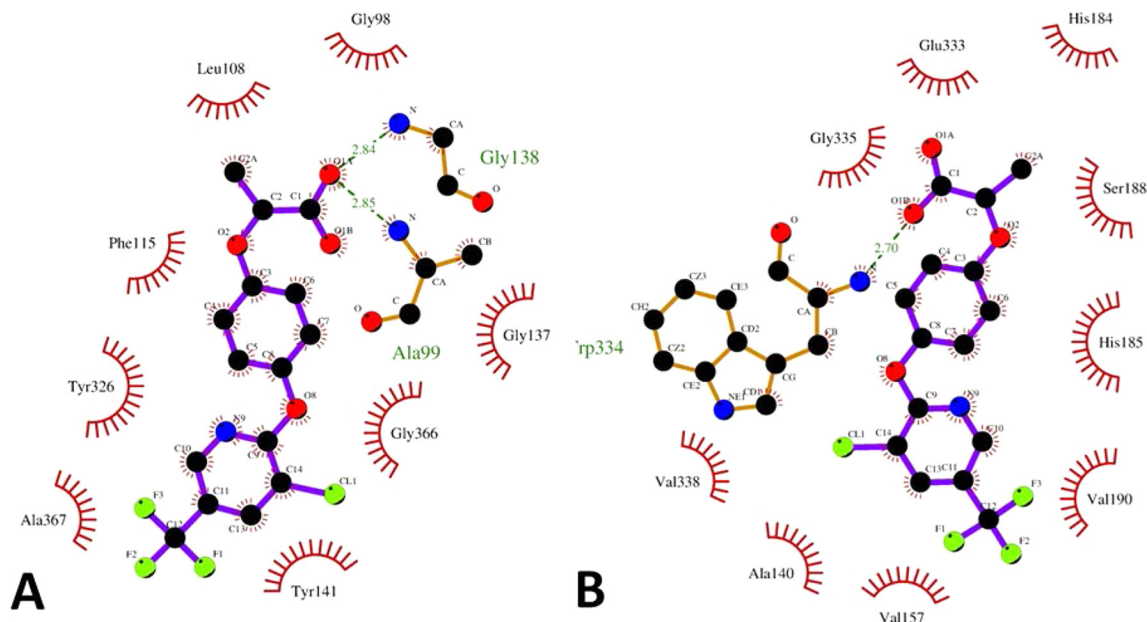
FIG 6 Haloxyfop interactions with residues on binding site 1 (A) and binding site 2 (B). Hydrogen bonds are depicted as green dashed lines, and hydrophobic interactions are depicted as red half circles.

and disrupts the oxyanion hole, where the haloxyfop central phenyl ring would prevent Gly131 from interacting with the acyl group. The haloxyfop carboxyl tail partially overlaps with the acyl tail position of the CoA substrate, competing with it for binding. Both the haloxyfop-bound structure and the apo structure have two channels accessing the active site: one that leads from the side closer to the CoA binding site and one that leads from the side closer to the biotin binding site (Fig. 7A). Haloxyfop binding site 1 (Fig. 7B) obstructs the CoA binding channel, while binding site 2 (Fig. 7C) obstructs the channel leading to the biotin-accommodating part of the pocket. Additionally, haloxyfop binding site 2 is formed by a set of residues unique to *M. tuberculosis* AccD6 that form a hydrophobic pocket: Trp334 (Asn1965 in yeast), His185 (Met1785 in yeast), His184 (Ile1782 in yeast), and Val338

(Leu1968 in yeast). Trp334 is perhaps the most essential residue in forming binding site 2 because not only does it form a wall of the pocket, but also its side chain packing allows the backbone to hydrogen bond to haloxyfop. Thus, the two haloxyfop binding sites may play a synergistic role in interfering with both substrate binding and product dissociation, resulting in a more potent inhibition than the proteins containing single haloxyfop binding sites seen in other species.

Isothermal titration calorimetry (ITC). The binding of the two haloxyfop-*R* molecules to *M. tuberculosis* AccD6 was further characterized by ITC measurements to determine the stoichiometry of interaction (n) and the dissociation constant (K_d). The ITC plot obtained from titration of haloxyfop-*R* is displayed in Fig. 8. Data were best fitted to the single-mode data analysis, giving an n
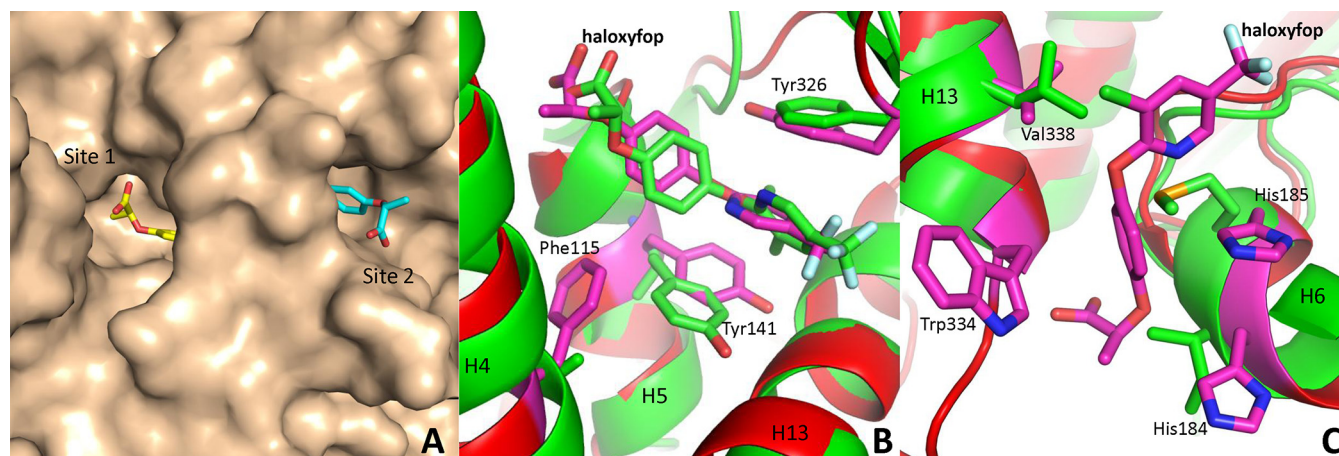

FIG 7 (A) Haloxyfop-*R* entry points to binding sites 1 and 2. A surface representation of AccD6 (tan) and the relationship of site 1 (haloxyfop in yellow) with site 2 (haloxyfop in cyan) is shown. Ligands are shown as sticks. (B and C) Comparison of the *M. tuberculosis* AccD6 and *S. cerevisiae* haloxyfop-binding sites. Protein is shown as ribbons, with haloxyfop and selected side chains shown as sticks and colored by element. (B) Haloxyfop site 1 superimposition. *M. tuberculosis* AccD6 is shown in purple, and the yeast CT domain is shown in green. (C) Haloxyfop site 2. *M. tuberculosis* AccD6 is in red, and the yeast CT domain is in green.
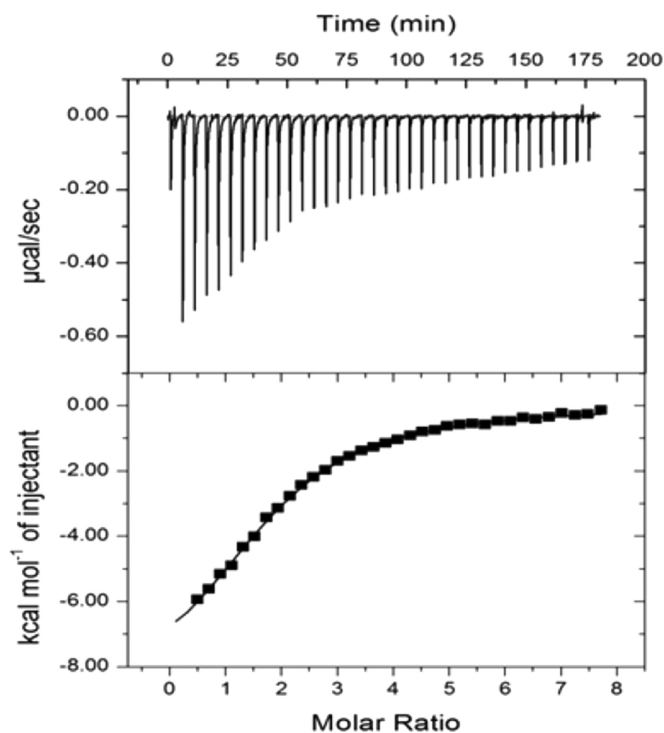
FIG 8 ITC curve of binding of haloxyfop-*R* to *M. tuberculosis* AccD6.

value of 1.83 ± 0.03 and a molar ratio of 2:1. The *n* value is consistent with the structural data of two molecules of haloxyfop-*R* bound per subunit. The K_d value of 35.8 ± 1.38 μM is in agreement with the IC_{50}. These results are indicative of the presence of two binding sites on each subunit; however, further experiments are necessary to determine whether these sites have equal affinities for haloxyfop-*R* and whether binding is cooperative. Besides the differences in the set of amino acids that compose each binding site, the interactions of haloxyfop at both binding sites 1 and 2 are highly similar when the H-bonding pattern and number of hydrophobic contacts are compared. These features might help to explain the best fit of data to the single binding mode.

The thermodynamic discrimination profile for haloxyfop-*R* binding ($\Delta H = -9,300$ cal/mol; $-T\Delta S = 3,122$ cal/mol/degree; $\Delta G = -6,177$ cal/mol) indicates that its interaction with AccD6 is mostly enthalpy driven (due to hydrogen bond donors' and acceptors' good placement on both binding sites [Fig. 6A and B] as well as favorable van der Waals interactions) and presents unfavorable entropy (due to haloxyfop-*R* flexibility and high polarity). Compounds with favorable enthalpy of binding have been described as good starting molecules for further drug development through entropic optimization by the addition of more hydrophobic groups (41), which can lead to highly selective tight-binding inhibitors (42).

The presence of two binding sites for haloxyfop raises two equally promising opportunities: (i) the development of high-affinity inhibitors capable of binding to both sites would likely reduce the emergence of resistance from single point mutations, and (ii) the spatial relationship of two binding sites allows the exploration of the channel that connects them. The addition of substituent groups that can interact with the amino acid side chains positioned in the connecting channel can improve binding by

exploring less specific hydrophobic contacts. These features are both related to inhibitors with a lower frequency of mutations that cause drug resistance (43).

***M. tuberculosis* AccD6 and AccD5 differences can explain haloxyfop-*R* selective inhibition of AccD6.** *M. tuberculosis* AccD6 shares 37% sequence identity with *M. tuberculosis* AccD5, with a 1.6-Å RMSD (Cα atoms). However, the oligomeric state of *M. tuberculosis* AccD6 is dimeric, while *M. tuberculosis* AccD5 is characterized as a hexamer in solution (8). As described above, *M. tuberculosis* AccD5 has been characterized as a propionyl-CoA carboxylase (12) and is not inhibited by haloxyfop (5). Comparison of *M. tuberculosis* AccD6 and AccD5 reveals that the selectivity is rooted in the portion of the haloxyfop binding cavity (site 1) that is occupied by the terminal acid of haloxyfop in the AccD6 structure (Fig. 9A). Haloxyfop is likely to be sterically blocked from binding to this region of AccD5, due to the larger side chain of Tyr167, which is Val111 in AccD6. In addition, the comparison of the structures of AccD6 with haloxyfop with apo-AccD5, shows that residue His195 (Ala139 in AccD6) and Tyr128 (Gly72 in AccD6) in AccD5 force Leu124 into the haloxyfop binding site, while the corresponding residue in AccD6 (Met68) does not extend into the binding pocket, which hinders haloxyfop binding. Ser163 of AccD5 also helps fill this portion of the haloxyfop site to a larger degree than the equivalent residue in AccD6 (Ala107) (Fig. 9A). AccD4, the third essential AccD for *M. tuberculosis* survival, is not inhibited by the FOP and DIM herbicides tested here (data not shown).

Structural analysis of *M. tuberculosis* AccD6 and yeast CT domain differential haloxyfop activity. Haloxyfop also binds to the yeast CT domain but displays much weaker *in vitro* inhibition activity (IC_{50} of ~500 μM for the yeast CT domain [40]). In order to uncover possible structural explanations for differences in inhibition, we further compared the binding mode of haloxyfop to *M. tuberculosis* AccD6 site 1 with that of the yeast CT domain (PDB code 1UYS) (19).

In both structures, the pyridyl ring is engaged in π-π stacking interactions with aromatic amino acids. However, the nature of the stacking rings is different (Fig. 7B and 9B). Tyr326, which stacks with the pyridyl ring, is a phenylalanine residue in the corresponding position of the yeast structure. The side chain oxygen atom of this tyrosine residue allows a larger degree of stabilization by means of a water-mediated hydrogen bond to the backbone nitrogen of Thr160 (2.9 Å from the tyrosine side chain oxygen atom to the water and 2.6 Å from the water to the backbone nitrogen of Thr160). In *M. tuberculosis* AccD6, the stacking interactions of Tyr326, the pyridyl ring, and Tyr141 form a more ideal interaction than the same stacking interactions in the yeast structure, where the pyridyl ring is tilted approximately 45° out of the plane formed by both aromatic side chains. The oxygen atom on the side chain of Tyr326 (compared to Phe1956 in the yeast structure) creates a more compact packing area around the ligand, which may be why it is 1.0 Å farther from this aromatic group in the *M. tuberculosis* AccD6 structure. Phe115 in the *M. tuberculosis* AccD6 structure is an alanine residue (Ala1712) in the corresponding position of the yeast CT domain. Consequently, Phe115 is positioned in such a way that Tyr141 is approximately 2 Å closer to haloxyfop, which allows a tighter stacking interaction in the *M. tuberculosis* site.

The haloxyfop trifluoromethyl group interactions differ between the two organisms (Fig. 9C). The *M. tuberculosis* AccD6
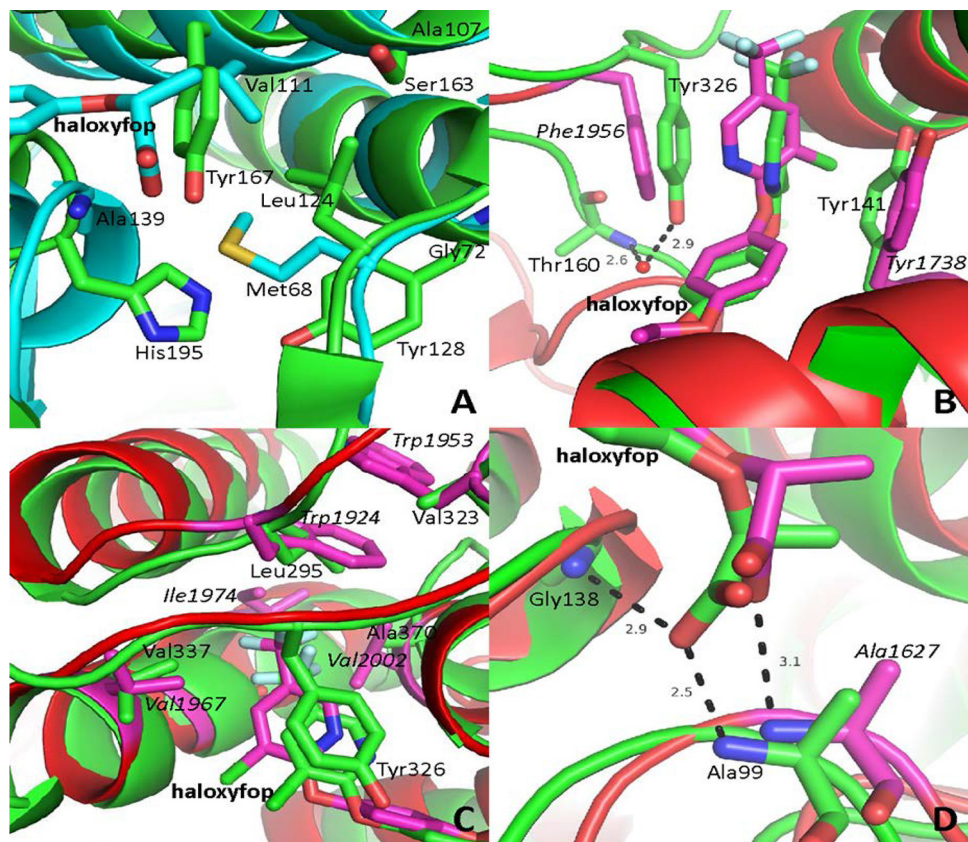
FIG 9 (A) Superimposition of *M. tuberculosis* AccD6 and AccD5. Cα RMSD, 1.6 Å. AccD6 is in blue and AccD5 (PDB code 2A7S) is in green. (B) Comparison of stacking interactions between *M. tuberculosis* AccD6 (green) and the yeast CT domain (red). (C) Comparison of the haloxyfop trifluoro methyl binding site. *M. tuberculosis* AccD6 site 1 is in green, and the yeast CT domain is in red. (D) Comparison of the hydrogen bonding at the acid position of haloxyfop. *M. tuberculosis* AccD6 site 1 is in green, and the yeast CT domain is in red. Yeast residue numbering is in italics.

trifluoromethyl group is surrounded by the side chains of the residues Tyr326, Ala370, Gly341, Val337, and Leu295, whereas the trifluoromethyl group in the yeast CT domain is packed around the side chains of Val1967, Trp1924, Val2002, Ile1974, and Gly1971. The most striking difference between the two structures in reference to the trifluoromethyl packing is the presence of the Trp1924 side chain in yeast and Leu295 in the corresponding position of *M. tuberculosis* AccD6. Not only does the indole side chain provide more packing surface area and a different electronic environment, it is also involved in a stacking interaction with another tryptophan residue side chain (Trp1953; Val323 in *M. tuberculosis* AccD6). Finally, the terminal acid group of haloxyfop is within hydrogen bonding distance of two atoms in the *M. tuberculosis* AccD6 structure (2.9 Å to the Gly138 backbone nitrogen atom and 2.5 Å to the Ala99 backbone nitrogen atom), whereas the yeast CT domain has a longer hydrogen bond (3.1 Å to Ala1627 backbone nitrogen atom) (Fig. 9D).

Conclusion. *M. tuberculosis* AccD6 is an attractive drug target because of its vital role in fatty acid biosynthesis (44). The results presented here demonstrate that haloxyfop is an inhibitor of *M. tuberculosis* AccD6. The AccD6-haloxyfop bound structure reveals a second binding site for the inhibitor on each subunit of the AccD6 dimer. The atomic structure of the enzyme-inhibitor complex provides detailed information of the binding mode for the further development of higher affinity inhibitors. Furthermore,

the proximity of both binding sites in each subunit, and the identification of a communicating channel, opens the possibility for experiments exploring these binding sites for improvements in both affinity and residency time of lead compounds.

REFERENCES

1. **Wakil SJ, Stoops JK, Joshi VC.** 1983. Fatty acid synthesis and its regulation. Annu. Rev. Biochem. **52**:537–579. http://dx.doi.org/10.1146/annurev.bi.52 .070183.002541.
2. **Cronan JE, Jr, Waldrop GL.** 2002. Multi-subunit acetyl-CoA carboxylases. Prog. Lipid Res. **41**:407–435. http://dx.doi.org/10.1016/S0163-7827 (02)00007-3.
3. **Tanabe T, Wada K, Okazaki T, Numa S.** 1975. Acetyl-coenzyme-A

carboxylase from rat liver. Subunit structure and proteolytic modification. Eur. J. Biochem. **57:**15–24.

4. **Cole ST, Brosch R, Parkhill J, Garnier T, Churcher C, Harris D, Gordon SV, Eiglmeier K, Gas S, Barry CE, Tekaia F, Badcock K, Basham D, Brown D, Chillingworth T, Conner R, Davies R, Devlin K, Feltwell T, Gentles S, Hamlin N, Holroyd S, Hornsby T, Jagels K, Krogh A, McLean J, Moule S, Murphy L, Oliver K, Osborne J, Quail MA, Rajandream MA, Rogers J, Rutter S, Seeger K, Skelton J, Squares R, Squares S, Sulston JE, Taylor K, Whitehead S, Barrell BG.** 1998. Deciphering the biology of *Mycobacterium tuberculosis* from the complete genome sequence. Nature **393:**537–544. http://dx.doi.org/10.1038/31159.

5. **Lin TW, Melgar MM, Kurth D, Swamidass SJ, Purdon J, Tseng T, Gago G, Baldi P, Gramajo H, Tsai SC.** 2006. Structure-based inhibitor design of AccD5, an essential acyl-CoA carboxylase carboxyltransferase domain of *Mycobacterium tuberculosis*. Proc. Natl. Acad. Sci. U. S. A. **103:**3072–3077. http://dx.doi.org/10.1073/pnas.0510580103.

6. **Sassetti CM, Boyd DH, Rubin EJ.** 2001. Comprehensive identification of conditionally essential genes in mycobacteria. Proc. Natl. Acad. Sci. U. S. A. **98:**12712–12717. http://dx.doi.org/10.1073/pnas.231275498.

7. **Takayama K, Wang C, Besra GS.** 2005. Pathway to synthesis and processing of mycolic acids in *Mycobacterium tuberculosis*. Clin. Microbiol. Rev. **18:**81–10. http://dx.doi.org/10.1128/CMR.18.1.81-101.2005.

8. **Holton SJ, King-Scott S, Nasser-Eddine A, Kaufmann SH, Wilmanns M.** 2006. Structural diversity in the six-fold redundant set of acyl-CoA carboxyltransferases in *Mycobacterium tuberculosis*. FEBS Lett. **580:**6898–6902. http://dx.doi.org/10.1016/j.febslet.2006.11.054.

9. **Sassetti C, Rubin EJ.** 2002. Genomic analyses of microbial virulence. Curr. Opin. Microbiol. **5:**27–32. http://dx.doi.org/10.1016/S1369-5274(02)00281-3.

10. **Sassetti CM, Boyd DH, Rubin EJ.** 2003. Genes required for mycobacterial growth defined by high density mutagenesis. Mol. Microbiol. **48:**77–84. http://dx.doi.org/10.1046/j.1365-2958.2003.03425.x.

11. **Daniel J, Oh TJ, Lee CM, Kolattukudy PE.** 2007. AccD6, a member of the Fas II locus, is a functional carboxyltransferase subunit of the acyl-coenzyme A carboxylase in *Mycobacterium tuberculosis*. J. Bacteriol. **189:**911–917. http://dx.doi.org/10.1128/JB.01019-06.

12. **Oh TJ, Daniel J, Kim HJ, Sirakova TD, Kolattukudy PE.** 2006. Identification and characterization of Rv3281 as a novel subunit of a biotin-dependent acyl-CoA carboxylase in *Mycobacterium tuberculosis*. J. Biol. Chem. **281:**3899–3908. http://dx.doi.org/10.1074/jbc.M511761200.

13. **Shaner DL.** 2004. Herbicide safety relative to common targets in plants and mammals. Pest Manag. Sci. **60:**17–24. http://dx.doi.org/10.1002/ps.782.

14. **Gronwald JW.** 1994. Herbicides inhibiting acetyl-CoA carboxylase. Biochem. Soc. Trans. **22:**616–621.

15. **Waller RF, Keeling PJ, Donald RGK, Striepen B, Handman E, Lang-Unnasch N, Cowman AF, Besra GS, Roos DS, McFadden GI.** 1998. Nuclear-encoded proteins target to the plastid in *Toxoplasma gondii* and *Plasmodium falciparum*. Proc. Natl. Acad. Sci. U. S. A. **95:**12352–12357. http://dx.doi.org/10.1073/pnas.95.21.12352.

16. **Zuther E, Johnson JJ, Haselkorn R, McLeod R, Gornicki P.** 1999. Growth of *Toxoplasma gondii* is inhibited by aryloxyphenoxypropionate herbicides targeting acetyl-CoA carboxylase. Proc. Natl. Acad. Sci. U. S. A. **96:**13387–13392. http://dx.doi.org/10.1073/pnas.96.23.13387.

17. **Nikolskaya T, Zagnitko O, Tevzadze G, Haselkorn R, Gornicki P.** 1999. Herbicide sensitivity determinant of wheat plastid acetyl-CoA carboxylase is located in a 400-amino acid fragment of the carboxyltransferase domain. Proc. Natl. Acad. Sci. U. S. A. **96:**14647–14651. http://dx.doi.org/10.1073/pnas.96.25.14647.

18. **Gornicki P, Haselkorn R.** 1993. Wheat acetyl-CoA carboxylase. Plant Mol. Biol. **22:**547–552. http://dx.doi.org/10.1007/BF00015984.

19. **Zhang H, Tweel B, Tong L.** 2004. Molecular basis for the inhibition of the carboxyltransferase domain of acetyl-coenzyme-A carboxylase by haloxyfop and diclofop. Proc. Natl. Acad. Sci. U. S. A. **101:**5910–5915. http://dx.doi.org/10.1073/pnas.0400891101.

20. **Xiang S, Callaghan MM, Watson KG, Tong L.** 2009. A different mechanism for the inhibition of the carboxyltransferase domain of acetyl-coenzyme A carboxylase by tepraloxydim. Proc. Natl. Acad. Sci. U. S. A. **106:**20723–20727. http://dx.doi.org/10.1073/pnas.0908431106.

21. **Yu LP, Kim YS, Tong L.** 2010. Mechanism for the inhibition of the carboxyltransferase domain of acetyl-coenzyme A carboxylase by pinoxaden. Proc. Natl. Acad. Sci. U. S. A. **107:**22072–22077. http://dx.doi.org/10.1073/pnas.1012039107.

22. **Guchhait RB, Polakis SE, Dimroth P, Stoll E, Moss J, Lane MD.** 1974. Acetyl coenzyme-A carboxylase system of *Escherichia coli*—purification and properties of biotin carboxylase, carboxyltransferase, and carboxyl carrier protein components. J. Biol. Chem. **249:**6633–6645.

23. **Rendina AR, Craigkennard AC, Beaudoin JD, Breen MK.** 1990. Inhibition of acetyl-coenzyme-A carboxylase by 2 classes of grass-selective herbicides. J. Agric. Food Chem. **38:**1282-1287. http://dx.doi.org/10.1021/jf00095a029.

24. **Otwinowski Z, Minor W.** 1997. Processing of X-ray diffraction data collected in oscillation mode. Method Enzymol. **276:**307–326. http://dx.doi.org/10.1016/S0076-6879(97)76066-X.

25. **Strong M, Sawaya MR, Wang SS, Phillips M, Cascio D, Eisenberg D.** 2006. Toward the structural genomics of complexes: crystal structure of a PE/PPE protein complex from *Mycobacterium tuberculosis*. Proc. Natl. Acad. Sci. U. S. A. **103:**8060–8065. http://dx.doi.org/10.1073/pnas.0602606103.

26. **McCoy AJ, Grosse-Kunstleve RW, Adams PD, Winn MD, Storoni LC, Read RJ.** 2007. Phaser crystallographic software. J. Appl. Crystallogr. **40:**658–674. http://dx.doi.org/10.1107/S0021889807021206.

27. **Emsley P, Cowtan K.** 2004. Coot: model-building tools for molecular graphics. Acta Crystallogr. D Biol. Crystallogr. **60:**2126–2132. http://dx.doi.org/10.1107/S0907444904019158.

28. **Chen VB, Arendall WB, III, Headd JJ, Keedy DA, Immormino RM, Kapral GJ, Murray LW, Richardson JS, Richardson DC.** 2010. MolProbity: all-atom structure validation for macromolecular crystallography. Acta Crystallogr. D Biol. Crystallogr. **66:**12–21. http://dx.doi.org/10.1107/S0907444909042073.

29. **DeLano WL.** 2004. Use of PYMOL as a communications tool for molecular science. Abstr. Pap. Am. Chem. Soc. **228:**U313–U314.

30. **Levert KL, Waldrop GL.** 2002. A bisubstrate analog inhibitor of the carboxyltransferase component of acetyl-CoA carboxylase. Biochem. Biophys. Res. Co. **291:**1213–1217. http://dx.doi.org/10.1006/bbrc.2002.6576.

31. **Secor J, Cseke C.** 1988. Inhibition of acetyl-CoA carboxylase activity by haloxyfop and tralkoxydim. Plant Physiol. **86:**10–12. http://dx.doi.org/10.1104/pp.86.1.10.

32. **Benning MM, Haller T, Gerlt JA, Holden HM.** 2000. New reactions in the crotonase superfamily: structure of methylmalonyl CoA decarboxylase from *Escherichia coli*. Biochemistry **39:**4630–4639. http://dx.doi.org/10.1021/bi9928896.

33. **Heinig M, Frishman D.** 2004. STRIDE: a web server for secondary structure assignment from known atomic coordinates of proteins. Nucleic Acids Res. **32:**W500–W502. http://dx.doi.org/10.1093/nar/gkh429.

34. **Claude JB, Suhre K, Notredame C, Claverie JM, Abergel C.** 2004. CaspR: a web server for automated molecular replacement using homology modeling. Nucleic Acids Res. **32:**W606–W609. http://dx.doi.org/10.1093/nar/gkh400.

35. **Rajamohan F, Marr E, Reyes AR, Landro JA, Anderson MD, Corbett JW, Dirico KJ, Harwood JH, Tu M, Vajdos FF.** 2011. Structure-guided inhibitor design for human acetyl-coenzyme A carboxylase by interspecies active site conversion. J. Biol. Chem. **286:**41510–41519. http://dx.doi.org/10.1074/jbc.M111.275396.

36. **Diacovich L, Mitchell DL, Pham H, Gago G, Melgar MM, Khosla C, Gramajo H, Tsai SC.** 2004. Crystal structure of the beta-subunit of acyl-CoA carboxylase: structure-based engineering of substrate specificity. Biochemistry **43:**14027–14036. http://dx.doi.org/10.1021/bi049065v.

37. **Arabolaza A, Shillito ME, Lin TW, Diacovich L, Melgar M, Pham H, Amick D, Gramajo H, Tsai SC.** 2010. Crystal structures and mutational analyses of acyl-CoA carboxylase beta subunit of Streptomyces coelicolor. Biochemistry **49:**7367–7376. http://dx.doi.org/10.1021/bi1005305.

38. **Bilder P, Lightle S, Bainbridge G, Ohren J, Finzel B, Sun F, Holley S, Al-Kassim L, Spessard C, Melnick M, Newcomer M, Waldrop GL.** 2006. The structure of the carboxyltransferase component of acetyl-coA carboxylase reveals a zinc-binding motif unique to the bacterial enzyme. Biochemistry **45:**1712–1722. http://dx.doi.org/10.1021/bi0520479.

39. **Diacovich L, Peiru S, Kurth D, Rodriguez E, Podesta F, Khosla C, Gramajo H.** 2002. Kinetic and structural analysis of a new group of acyl-CoA carboxylases found in *Streptomyces coelicolor* A3(2). J. Biol. Chem. **277:**31228–31236. http://dx.doi.org/10.1074/jbc.M203263200.

40. **Zhang H, Yang Z, Shen Y, Tong L.** 2003. Crystal structure of the carboxyltransferase domain of acetyl-coenzyme A carboxylase. Science **299:**2064–2067. http://dx.doi.org/10.1126/science.1081366.

41. **Lafont V, Armstrong AA, Ohtaka H, Kiso Y, Amzel LM, Freire E.** 2007. Compensating enthalpic and entropic changes hinder binding affinity op-

timization. Chem. Biol. Drug Des. **69:**413–422. http://dx.doi.org/10.1111 /j.1747-0285.2007.00519.x.

42. **Velazquez-Campoy A, Todd MJ, Freire E.** 2000. HIV-1 protease inhibitors: enthalpic versus entropic optimization of the binding affinity. Biochemistry **39:**2201–2207. http://dx.doi.org/10.1021/bi992399d.

43. **Ohtaka H, Schön A, Freire E.** 2003. Multidrug resistance to HIV-1 protease inhibition requires cooperative coupling between distal mutations. Biochemistry **42:**13659–13666. http://dx.doi.org/10.1021/bi0350405.

44. **Glickman MS, Cox JS, Jacobs WR.** 2000. A novel mycolic acid cyclopropane synthetase is required for cording, persistence, and virulence of *Mycobacterium tuberculosis*. Mol. Cell **5:**717–727. http://dx.doi.org/10.1016 /S1097-2765(00)80250-6.

Antimicrobial Agents and Chemotherapy